Evidence for a floating phase of the transverse ANNNI model at high frustration

Matteo Beccaria,[1,*] Massimo Campostrini,[2,†] and Alessandra Feo[3,‡]
[1]*Dipartimento di Fisica dell'Università di Lecce and INFN, Sezione di Lecce, Via Arnesano, 73100 Lecce, Italy*
[2]*Dipartimento di Fisica dell'Università di Pisa and INFN, Sezione di Pisa, Largo Bruno Pontecorvo 3, 56127 Pisa, Italy*
[3]*Dipartimento di Fisica dell'Università di Parma and INFN, Gruppo Collegato di Parma, Viale G. P. Usberti 7/A, 43100 Parma, Italy*
(Received 6 March 2007; revised manuscript received 29 May 2007; published 20 September 2007)

We study the transverse quantum ANNNI model in the region of high frustration ($\kappa > 0.5$) using the density matrix renormalization group algorithm. We obtain a precise determination of the phase diagram, showing clear evidence for the existence of a floating phase, separated from the paramagnetic modulated phase by a high-order critical line ending at the multicritical point. We obtain simple and accurate formulas for the two critical lines.

DOI: 10.1103/PhysRevB.76.094410 PACS number(s): 75.10.Jm, 73.43.Nq, 05.10.Cc

I. MODEL

The ANNNI model is an axial Ising model with competing next-nearest-neighbor antiferromagnetic coupling in one direction. It is a paradigm for the study of competition between magnetic ordering, frustration, and thermal disordering effects.

In the Hamiltonian limit, we consider a one-dimensional quantum spin $S=\frac{1}{2}$ chain interacting with an external magnetic field, called the TAM model (transverse ANNNI).

The TAM Hamiltonian for L spins with open boundary conditions reads[1,2]

$$H = -J_1 \sum_{i=1}^{L-1} \sigma_i^z \sigma_{i+1}^z - J_2 \sum_{i=1}^{L-2} \sigma_i^z \sigma_{i+2}^z - B \sum_{i=1}^{L} \sigma_i^x. \tag{1}$$

We use the "traditional" notation $\kappa = -J_2/J_1$. The notations $\lambda = J_1/B$ and $\Gamma = B$ are sometimes used in the literature.

The sign of J_1 is immaterial, since the Hamiltonian is invariant under the transformation

$$J_1 \to -J_1, \quad \sigma_i^y \to (-1)^i \sigma_i^y, \quad \sigma_i^z \to (-1)^i \sigma_i^z. \tag{2}$$

Likewise, the sign of B is immaterial. Without loss of generality, we set $J_1 = 1$. We restrict ourselves to positive κ and even L.

We also consider fixed boundary conditions, where we add to the extremities of the chain two fixed spins σ_0 and σ_{L+1}, with the possibilities of parallel $(\sigma_0, \sigma_{L+1} = \uparrow\uparrow)$ or antiparallel $(\sigma_0, \sigma_{L+1} = \uparrow\downarrow)$ boundary conditions.

In the region of high frustration ($\kappa > 0.5$), despite extensive studies,[3–7] the phase diagram of the transverse ANNNI model is not well known. For low B, the model is known to be in the gapless "antiphase" $\uparrow\uparrow\downarrow\downarrow$. It undergoes a second-order phase transition at a magnetic field $B_1(\kappa)$. The existence of a "floating" phase, massless, and with slowly decaying spin correlation functions, up to a Kosterliz-Thouless phase transition at a magnetic field $B_2(\kappa)$, is an open question. For high B, the TAM is known to be in a paramagnetic modulated phase.

II. OBSERVABLES

We measure the two lowest energies E_0 and E_1, the mass gap $\Delta = E_1 - E_0$, the entanglement entropy S_A (see below), and two spin-spin correlation functions: the "slow" correlation function

$$c_s(d) = \langle \sigma_{L/2+1}^z \sigma_{L/2+1+d}^z \rangle, \quad 1 \le d \le L/2 \tag{3}$$

and the "fast" correlation function[16]

$$c_f(d) = \langle \sigma_{L/2-d}^z \sigma_{L/2+1+d}^z \rangle, \quad 0 \le d \le L/2. \tag{4}$$

Interesting quantities related to the correlation functions are as follows: The overlap o of $c_s(d)$ with the antiphase correlation function,

$$c_a(d) = (-1)^{\lfloor (d-L/2)/2 \rfloor}, \quad o = \frac{2}{L} \sum_{d=1}^{L/2} c_s(d) c_a(d). \tag{5}$$

The average fast correlation function (times an oscillating sign),

$$\bar{c}_f = (-1)^{L/2} \frac{2}{L+2} \sum_{d=0}^{L/2} c_f(d). \tag{6}$$

The range of the fast correlation function,

$$R = \frac{\sum_{d=0}^{L/2} d c_f^2(d)}{\sum_{d=0}^{L/2} c_f^2(d)}. \tag{7}$$

A. Entanglement entropy

It is possible to study an order-disorder phase transition using the entanglement entropy.[8] We divide the system of size L into a left subsystem of size ℓ and a right subsystem of size L-ℓ, and define

$$S_A(\ell; L) = -\mathrm{Tr}(\rho_A \ln \rho_A), \tag{8}$$

where A denotes the degrees of freedom of the left subsystem, B the degrees of freedom of the right subsystem, and $\rho_A = \mathrm{Tr}_B |\Psi_0\rangle\langle\Psi_0|$; note that $S_A(\ell; L) = S_A(L-\ell; L)$. For a critical system, we expect (neglecting lattice artifacts)

$$S_A(\ell;L) \sim (c/6)\log[L\sin(\pi\ell/L)], \tag{9}$$

where c is the conformal anomaly number (central charge) of the corresponding conformal field theory, and $\sim$ means "up to a (nonuniversal) additive constant;" for the case of interest for the infinite-volume DMRG, $\ell=\frac{1}{2}L$, and $\sin(\pi\ell/L)$ only shifts the additive constant. For a noncritical system, we expect

$$S_A\left(\frac{1}{2}L;L\right) \sim (c/6)[\log L + s(L/\xi)], \tag{10}$$

where $s(x)$ is a *universal* finite-size scaling function satisfying the constraints $s(0)=0$ and $s(x)\sim -\log x$ for large x.

B. Domain-wall energy

So far, we only considered open boundary conditions. Following Ref. 9, we define the domain-wall energy (note that our definition of L differs by 2 from the definition of Ref. 9)

$$E_{\mathrm{DW}}(\kappa,B,L) = (-1)^{L/2+1}[E_0^{\uparrow\uparrow}(\kappa,B,L) - E_0^{\uparrow\downarrow}(\kappa,B,L)], \tag{11}$$

where $E_0^{\uparrow\uparrow}$ and $E_0^{\uparrow\downarrow}$ are the ground state energies with parallel and antiparallel boundary conditions, respectively.

III. ALGORITHM

We implement the density matrix renormalization group (DMRG) algorithm described in Ref. 10. We sample the n_s lowest energy levels with equal weights, i.e., we use the reduced density matrix

$$\hat{\rho}_S = \frac{1}{n_s}\mathrm{Tr}_E \sum_{i=0}^{n_s-1} |\psi_i\rangle\langle\psi_i| \tag{12}$$

[see Eq. (26) of Ref. 10]. Usually, since we are interested in the mass gap Δ, we set $n_s=2$. We identify system and environment (for antiparallel boundary conditions, up to a spin flip $\sigma_i^y\to-\sigma_i^y$, $\sigma_i^z\to-\sigma_i^z$). The typical dimensions of the truncated system and environment M range from 80 to 160; in the following, $M=80$ will be understood, unless M is explicitly quoted.

The crucial part of the numerical computation is finding the lowest eigenvalues and eigenvectors of the superblock Hamiltonian; we employ the implicitly restarted Arnoldi algorithm implemented in ARPACK,[11] in the routine dsaupd used in mode 1. We use (typically) 100 Lanczos vectors and require convergence to machine precision, obtaining residual norms $|Hx-\lambda x|/|\lambda|\sim 10^{-14}$.

We observe a truncated weight (the sum of the eigenvalues of the density matrix whose eigenvectors are dropped in the truncation) $\varepsilon\sim 10^{-8}$ for "normal" configurations, and $\varepsilon\sim 10^{-7}$ for peaks of Δ (see below).

We managed to diagonalize the system exactly up to $L=22$; both the finite- and the infinite-volume DMRG algorithms, reproduce the results of exact diagonalization. For moderate L, finite- and the infinite-volume DMRGs, give consistent results. For higher L, discrepancies between finite- and infinite-volume DMRGs, and M dependence of Δ become noticeable; they are strongly observable dependent, and they will be discussed below, where results on observables are presented.

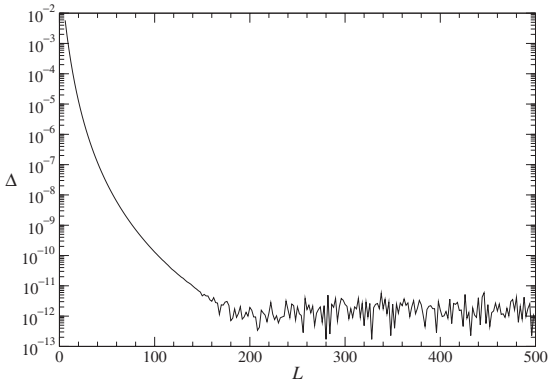

FIG. 1. Mass gap vs L for $\kappa=0.75$ and $B=0.257$. To appreciate the effect of numerical errors, note that $E_0(B=0.257)\cong -0.8L$.

During a run of the finite-volume DMRG algorithm on a system with L_n sites, information about the system and environment for all smaller system is available. It is therefore possible, with a moderate extra numerical effort, to estimate the observables for all the systems with $L<L_n$ sites. These estimates almost coincide with the results obtained running independently at each L. The additional errors introduced by this procedure will also be discussed below.

The finite-volume DMRG algorithm at large L requires a very large amount of memory; however, since the observables at each lattice size are accessed only twice per cycle, they can be conveniently kept on disk, requiring only a very large amount of disk space; for $L=600$ and $M=80$, e.g., $\sim$6 Gbytes are required.

IV. PHASES AT $\kappa=0.75$

We will first focus our attention on the model at $\kappa=0.75$, and later on extend the study to other values of κ.

Running the infinite-volume DMRG algorithm at $\kappa=0.75$ and $B\leqslant 0.257$, with open boundary conditions, we observe that the mass gap Δ vanishes exponentially in L, apart from numerical errors due to the fact that Δ is computed as E_1-E_0: see, e.g., Fig. 1.

The slow correlation function $c_s(d)$ almost coincides with $c_a(d)$; the overlap o approaches a value very close to 1 with corrections proportional to $1/L$. The fast correlation function $c_f(d)$ is constant and close to ± 1, apart from $d=0$ and d's close to $L/2$; the range R is almost exactly $L/4$ [the value for a constant $c_f(d)$] and the average $\bar{c}_f$ approaches a value very close to -1 with corrections proportional to $1/L$.

There is a very sharp phase transition at $0.257<B_1<0.258$. We will postpone its detailed study, since it is best done using E_{DW}.

Running at $\kappa=0.75$ and $B\geqslant 0.258$, the mass gap Δ as a function of L at fixed B shows sharp peaks with a frequency increasing with B: see Fig. 2. Each peak matches exactly a change of sign of $\bar{c}_f$. At each B, for L smaller than the first

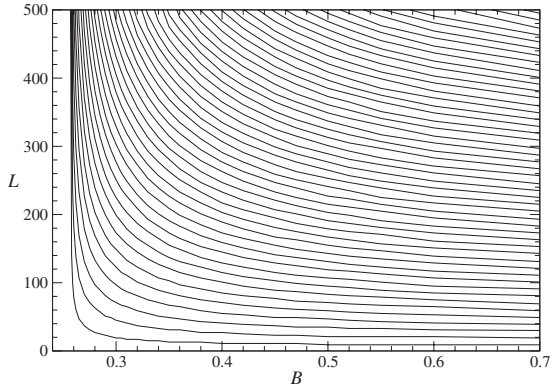

FIG. 2. Mass gap peaks in the L-B plane for $\kappa=0.75$.

peak, we observe signals very similar to the case $B \leqslant 0.257$; for higher L, we observe that the minima of Δ seem to go to zero for $B \leqslant 0.4$ and to a nonzero limit for $B \geqslant 0.5$; however, the determination of Δ from the infinite-volume DMRG is not accurate for $L \gtrsim 200$; finite-volume DMRG data with $M=80$ become unreliable for $L>300$; we show in Fig. 3 the case $B=0.3$.

We performed a finite-size analysis of Δ, similar to the analysis of Ref. 2, but with a complication arising from the peak structure. We run the finite-volume DMRG algorithm for $B=0.4, 0.41, 0.42, 0.43, 0.44, 0.45, 0.46$ and $L_n \geqslant 292$ corresponding to a minimum of Δ. For each B, we select the minima of Δ and define $\Delta_L(B,\kappa)$ outside the minima by interpolation in L. We now take two values L_1 and L_2 and look for the intersection $B_i(L_1,L_2)$ of the two curves $L_1\Delta_{L_1}(B,\kappa)$ and $L_2\Delta_{L_2}(B,\kappa)$ vs B (interpolating in B at fixed L and κ as needed). The results are shown in Fig. 4: we note that $M=120$ and $M=160$ data almost coincide, and even $M=80$ data are adequate in the range of L's considered; we quote as a final result $B_2=0.424(3)$. The data presented here were obtained from a run at a single L_n for each B (see Sec. III); in order to check that the error introduced is under control, we also performed separate runs for all the values of L required, for $N=80$ and for $N=120$ at $B=0.42$, and repeated the analysis: the values of $B_i(L_1,L_2)$ never change by more than 0.0005.

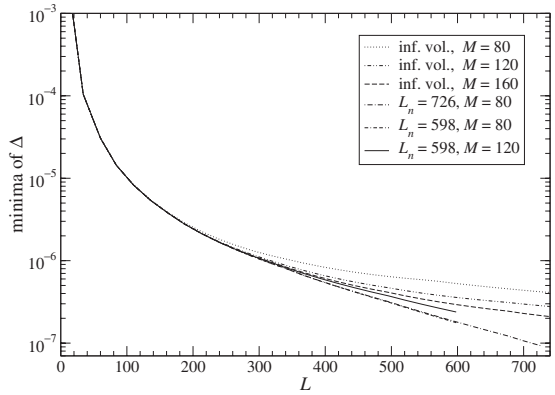

FIG. 3. Minima of mass gap Δ vs L for $\kappa=0.75$ and $B=0.3$.

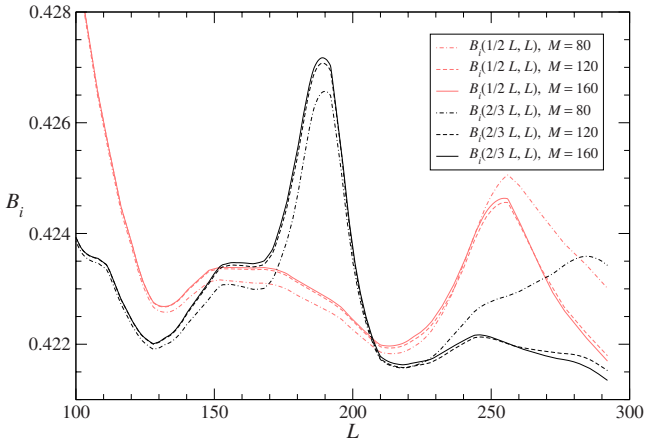

FIG. 4. (Color online) The intersection B_i vs L, for $\kappa=0.75$.

For $0.258 \leqslant B \lesssim 0.45$, the slow correlation function $c_s(d)$ at fixed L shows oscillations with power-law damping, in rough agreement with

$$c_s(d) \cong a d^{-\eta} \cos(qd+\phi), \tag{13}$$

with $\eta \sim 0$ for $B=0.258$, increasing with B but remaining smaller than $\frac{1}{3}$. For $B \gtrsim 0.5$, $c_s(d)$ at fixed L shows oscillations with exponential damping. We tried to extract η by fitting $c_s^2(d)$, smoothed by taking a running average over $\lfloor 2\pi/q + \frac{1}{2} \rfloor$ points, to the form $a d^{-2\eta}$. In Fig. 5, we show the typical case $B=0.425$; $c_s^2(d)$ for different values of L converge not to a single curve but to two separate curves, with different values of η, preventing a precise determination of η.

The range of the fast correlation function R should distinguish clearly the floating phase, where $R \to \infty$ as $L \to \infty$ (since $\eta < \frac{1}{2}$), from the paramagnetic phase, where R has a finite limit as $L \to \infty$. A first problem is the presence of oscillations,

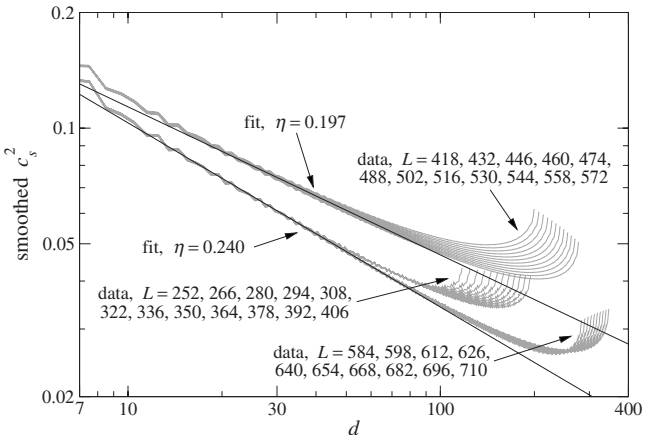

FIG. 5. The smoothed squared slow correlation function $c_s^2(d)$ for $\kappa=0.75$ and $B=0.425$, from the finite-volume DMRG at $L_n=710$ and $M=120$, for values of L corresponding to minima of Δ. (Data at $M=80$ give a very similar plot.)

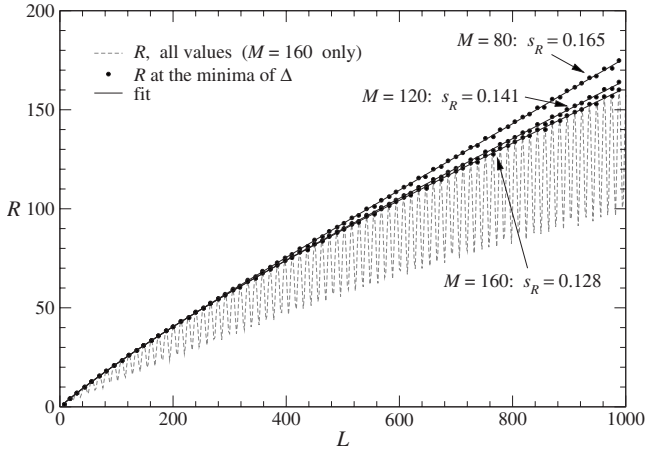

FIG. 6. R, at the L's corresponding to minima of Δ, with fits to Eq. (14), for $\kappa=0.75$, $B=0.45$, and different M's. For $M=160$, all the values of R are also plotted.

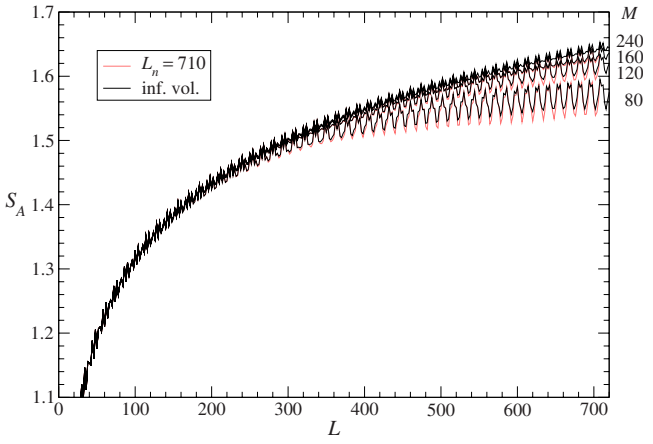

FIG. 7. (Color online) The entanglement entropy $S_A(\frac{1}{2}L;L)$ vs the size of the system L, for $\kappa=0.75$, $B=0.425$, $L_n=710$, and infinite-volume DMRG.

with dips corresponding to the peaks of Δ (see Fig. 6); it is solved by selecting the values of R at the L's corresponding to the peaks of Δ. After this operation, R vs L at fixed B and M is well fitted to the form

$$R(L) = \frac{s_R L^2 + pL}{L + q}. \tag{14}$$

If we plot the asymptotic slope s_R vs B, we should be able to see a drop toward 0 in correspondence with the phase transition. However, in the critical region, R (and s_R) strongly depend on M: see Fig. 6; we can only conclude that $B_2 \simeq 0.45$.

The analysis of the range of the slow correlation function gives similar, but even less precise, results. We conclude that the spin correlation functions are unsuitable for the precise determination of the floating/paramagnetic phase transition.

A. Entanglement entropy

We show in Fig. 7 the entanglement entropy S_A for the typical case $B=0.425$. Finite-volume DMRG essentially reproduces the results of infinite-volume DMRG at the same M. We can estimate that the DMRG determination of S_A is reliable up to $L=200$ for $M=80$, up to $L=300$ for $M=120$, and up to $L=400$ for $M=160$. For each value of M, within the given range of L, the difference between finite- and infinite-volume DMRG results is less than 0.001. We can therefore compute S_A using the faster infinite-volume DMRG, and this allows us to work at larger values of M.

In the antiphase, S_A is essentially constant, indicating a very small correlation length.

The simple ansatz for the finite-size scaling function entering Eq. (10),

$$s(x) = -\ln(x + e^{-\alpha x}), \tag{15}$$

with $\alpha \equiv 1$, is found to fit the entanglement entropy data very well (excluding just the very smallest lattices with $L \lesssim 10$) in all cases for the floating and paramagnetic phases; c is always compatible with 1. The best determination of ξ, obtained by fitting S_A with $c \equiv 1$ fixed, is shown in Fig. 8; our final estimate is $B_2=0.44(1)$.

B. Domain-wall energy

So far, we only considered open boundary conditions. We now switch to fixed boundary conditions, in order to compute the domain-wall energy $E_{\rm DW}$; with fixed boundary conditions, there are no problems with quasidegenerate energy levels (typically, $\Delta > 0.01$) or peaks in Δ associated with level crossings, and truncated weights are $\varepsilon \sim 10^{-9}$ or smaller for $M=80$. Even if we are not interested in the mass gap, we run with $n_s=2$, which gives results more stable than $n_s=1$.

We may fit $E_{\rm DW}$ to the form

$$E_{\rm DW} = a \exp(-dL) L^{-\nu} + E_\infty \tag{16}$$

in the antiphase and

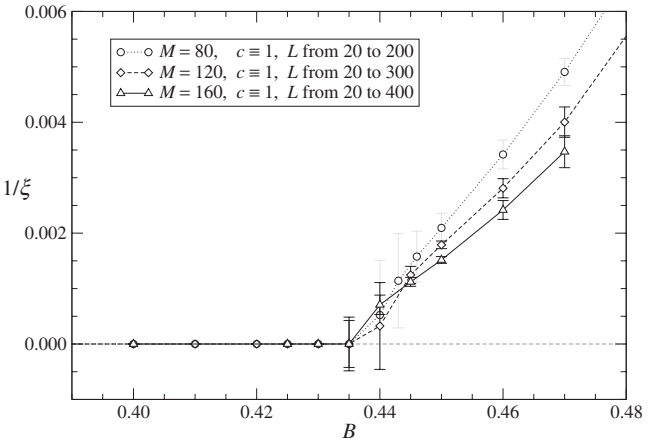

FIG. 8. The reciprocal correlation length $1/\xi$ (determined from S_A) vs B, for $\kappa=0.75$. Fitting the $M=120$ and $M=160$ data for $20 \leqslant L \leqslant 200$, we obtain results almost identical to the $M=80$ results plotted; likewise, fitting the $M=160$ data for $20 \leqslant L \leqslant 300$, we obtain results almost identical to the $M=120$ results plotted; we omit these results from the plot for readability. All data for $B \leqslant 0.43$ are consistent with zero, with a very small error ($\sim 10^{-6}$) which is not visible at the scale of the plot.

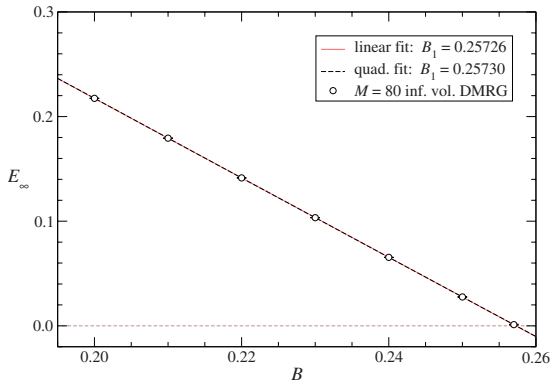

FIG. 9. (Color online) The infinite-volume domain-wall energy E_∞ vs B, for $\kappa=0.75$.

$$E_{\mathrm{DW}} = \frac{a\exp(-dL)}{L}[|\cos(kL+\phi)| - |\sin(kL+\phi)|] \qquad (17)$$

in the floating phase (with $d=0$) and in the paramagnetic phase.[9] The fits, excluding (typically) lattices with $L<16$, are of very good quality and stable.

Equation (16) fits perfectly E_{DW} for $B \leqslant 0.257$, giving $E_\infty \to 0$, constant $\nu \simeq 1.6$, and $d \simeq 0.008$ for $B \nearrow B_1$. Equation (17), with $d=0$, fits perfectly E_{DW} for $B>0.257$ and gives $k \to 0$ for $B \searrow B_1$. The best estimators of B_1 are E_∞ in the antiphase and k^2 in the floating phase, both vanishing linearly at B_1, see Figs. 9 and 10 and 10; the final estimate of the critical field is $B_1=0.2574(2)$.

So far, we obtained results very similar to those of Ref. 9. We turn now to the problem of identifying the floating phase, i.e., a region with $d=0$. The data generated with the infinite-volume DMRG at $0.3<B<0.4$ seem to indicate $d<0$; this appears to be an artifact of the infinite-volume DMRG, as we can see from the comparison of E_{DW} evaluated with the finite- and infinite-volume DMRG at $B=0.3$, shown in Fig. 11.

We must therefore resort to the resource-consuming finite-volume DMRG. We checked in several instances that

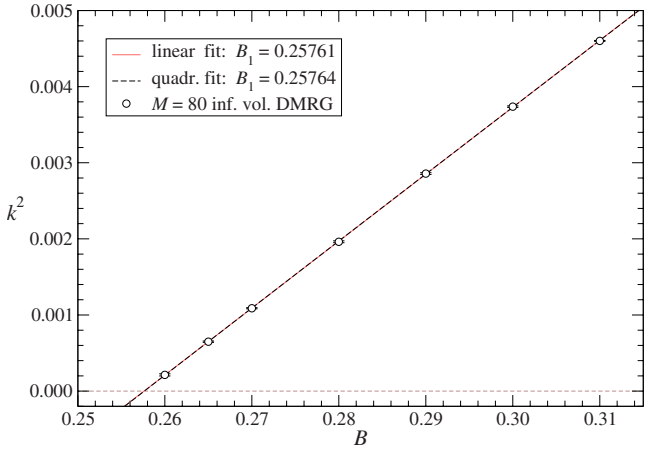

FIG. 10. (Color online) The squared modulation parameter k^2 vs B, for $\kappa=0.75$.

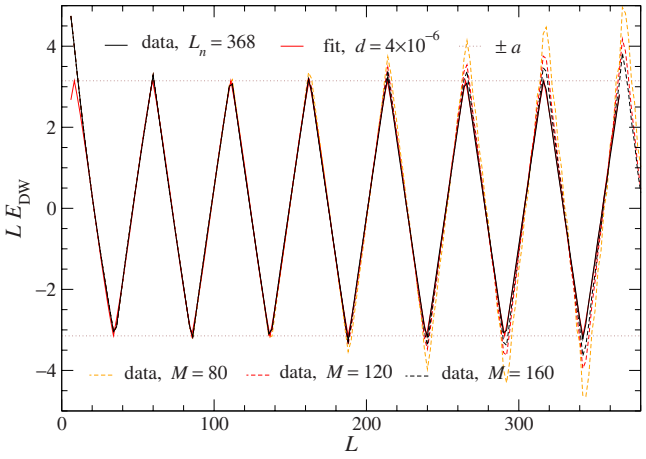

FIG. 11. (Color online) Determinations of the domain-wall energy E_{DW}, multiplied by L, vs L, for $\kappa=0.75$ and $B=0.3$: finite-volume DMRG at $M=80$, 120, 160; infinite-volume DMRG at $L_n=368$, $M=80$; fit to Eq. (17) of the $L_n=368$ data.

$M=80$ is sufficient to obtain accurate results and that obtaining the data for all L's from a run at a single L_n is acceptable: in all cases, the determinations of d are well within the error quoted.

We show the results in Fig. 12. The value of d obtained from the finite-volume DMRG is consistent with zero up to $B=0.425$, where we estimate $\xi \equiv 1/d > 10^4$. The smoothness of d vs B suggest a higher-order, possibly Kosterliz-Thouless, phase transition. Note that d is quite compatible with $1/\xi$ of Fig. 8 (apart from a normalization stemming from the different definition of correlation length), and so is the resulting $B_2=0.435(10)$.

The precise determination of the transition point of a Kosterliz-Thouless phase transition is a notoriously difficult problem: it is always possible that a system with a huge correlation length is mistaken for a critical system.[12] Indeed, the correlation length is expected to diverge very rapidly when the Kosterliz-Thouless critical coupling is approached; following Ref. 13, we could conjecture a behavior

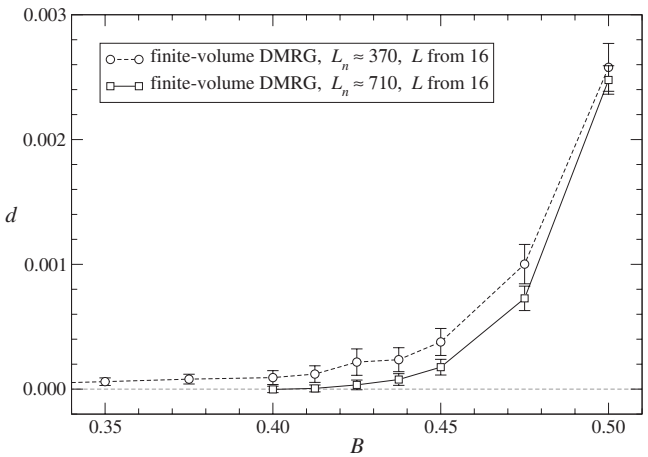

FIG. 12. The decay parameter d of the domain-wall energy E_{DW}, computed with the finite-volume DMRG, vs B, for $\kappa=0.75$.

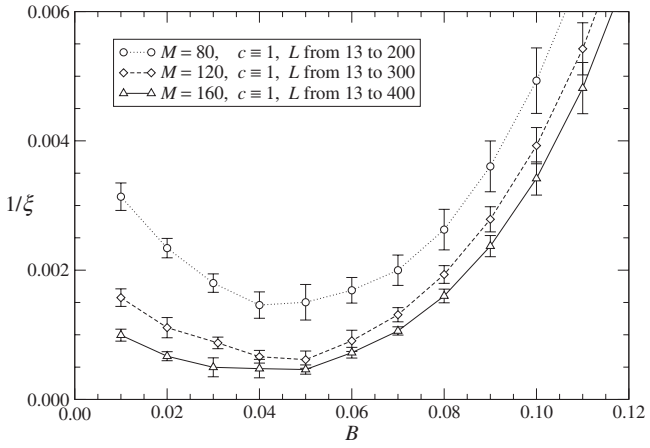

FIG. 13. The reciprocal correlation length $1/\xi$ (determined from S_A) vs B, for $\kappa=0.5$.

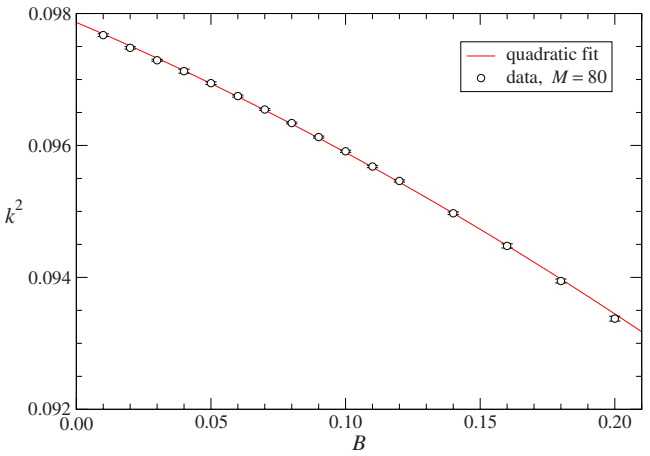

FIG. 14. (Color online) The squared modulation parameter k^2 vs B, for $\kappa=0.5$.

$\xi \propto \exp[b/(B-B_2)]$ for $B \searrow B_2$. A fit to the above form of the data of Fig. 12 gives unstable results for B_2, indicating that the determination of B_2 from $E_{\rm DW}$ should be treated with some caution. On the other hand, a fit to the data of Fig. 8 gives results which are stable and fully consistent with the estimate of B_2 from S_A given above.

The two determinations of B_2 from Δ_L and S_A, obtained by quite different methods, are accurate and in agreement with each other (and with the less reliable determination from $E_{\rm DW}$); moreover, for each method, we see no trend of B_2 decreasing with increasing L or M (see especially Figs. 4 and 8). We can conclude that, while it is possible that the errors on B_2 are underestimated, it is difficult to believe that the floating phase might disappear completely on larger systems.

V. PHASE DIAGRAM

The study of the phase transitions at other values of κ's is very similar to the one at $\kappa=0.75$ presented in Sec. IV and we can avoid repeating the details. We selected for our analysis the values $\kappa=0.5$, 0.52, 0.55, 0.6, 0.75, 1.0, 1.25, 1.5, 2.0, 5.0.

At $\kappa=0.5$, the DMRG algorithm becomes inefficient at low B, and we are unable to run at $B<0.01$. We see no sign of a floating phase: the curves $L\Delta_L(B,\kappa)$ vs B almost coincide for $B<0.06$, and the intersections are very unstable. Determining ξ by fitting S_A with $c\equiv 1$ fixed, we see no sign of $\xi=\infty$, see Fig. 13; given the poor convergence in M for small B, we estimate $B_2<0.04$. The analysis of $E_{\rm DW}$ does not give precise results for B_2. The behavior of the modulation parameter k (see Fig. 14), which goes to a nonzero value as $B\to 0$, hints at the very peculiar nature of the multicritical point at $\kappa=0.5$, $B=0$.[1,14]

For $\kappa=0.52$ and 0.55, the quality of the determinations of B_1 and of the determination of B_2 from S_A is similar to those at $\kappa=0.75$; on the other hand, the analysis of Δ_L and $E_{\rm DW}$ do not give precise results for B_2. We present the plot of $1/\xi$ for $\kappa=0.52$ in Fig. 15: the difference from Fig. 13 is remarkable.

For $0.6\leqslant\kappa\leqslant 1.5$, there are no relevant differences from the case $\kappa=0.75$ described in Sec. IV; we only present the determinations of B_1 and B_2 in Table I. For $\kappa=2$, the only difference is that $E_{\rm DW}$ is not fitted well by Eq. (17) in the floating and paramagnetic phases, and therefore the determination of B_2 from $E_{\rm DW}$ is unreliable.

In the case $\kappa=5$, the determination of B_1 and B_2 is rather imprecise: $E_{\rm DW}$ is not fitted well by Eq. (16) in the antiphase,

TABLE I. Determinations of the transition fields B_1 and B_2 by different techniques.

κ	B_1 ($E_{\rm DW}$)	B_1 (o)	B_2 (Δ_L)	B_2 (S_A)	B_2 ($E_{\rm DW}$)
0.5	0	0	<0.06	<0.04	<0.08
0.52	0.0201(1)	0.021(1)	0.095(15)	0.115(5)	0.12(3)
0.55	0.0501(2)	0.052(2)	0.160(15)	0.175(5)	0.18(2)
0.6	0.1015(2)	0.103(2)	0.235(6)	0.25(1)	0.25(1)
0.75	0.2574(2)	0.2575(5)	0.424(3)	0.44(1)	0.425(10)
1.0	0.5213(2)	0.522(2)	0.700(5)	0.72(1)	0.71(1)
1.25	0.7867(2)	0.785(2)	0.972(4)	1.00(1)	0.98(1)
1.5	1.0514(2)	1.045(5)	1.235(3)	1.26(1)	1.26(1)
2.0	1.5775(2)	1.576(2)	1.756(6)	1.79(1)	1.79(3)
5.0		4.667(3)		4.88(1)	

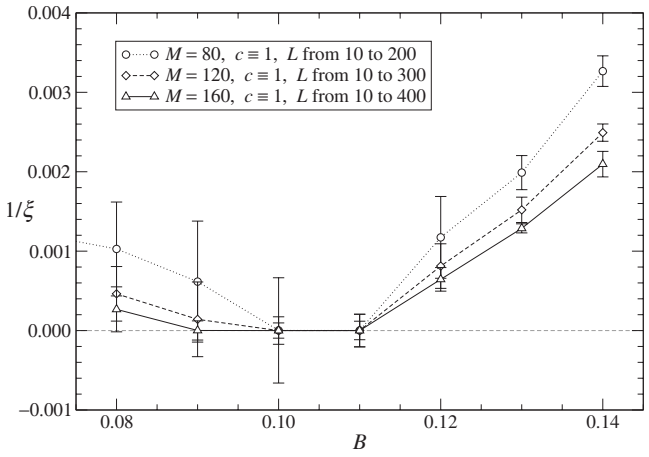

FIG. 15. The reciprocal correlation length $1/\xi$ (determined from S_A) vs B, for $\kappa=0.52$.

and it is fitted poorly by Eq. (17) in the floating and paramagnetic phases; it is very hard to get precise results from Δ_L, since the modulation parameter is very small ($k \lesssim 0.01$ in the floating phase). It is still possible to estimate B_1 from o and B_2 from S_A.

For all the values of κ considered, the different determinations of B_1 and B_2 are in substantial agreement with each other: this is a strong argument supporting the reliability of our results. It should be noticed, however, that the determination of B_2 from Δ_L is systematically lower than the determination from S_A, possibly indicating that the error on the determination from Δ_L reported in Table I is underestimated.

We can beautifully summarize all the above results by noticing that all the determinations of B_1 and B_2 are consistent with

$$B_1(\kappa) \cong 1.05\left(\kappa - \frac{1}{2}\right), \quad B_2(\kappa) \cong 1.05\sqrt{\left(\kappa - \frac{1}{2}\right)(\kappa - 0.1)}. \tag{18}$$

Finally, we draw the phase diagram in the κ-B plane in Fig. 16. The region $\kappa < 0.5$ was studied in Ref. 2; the critical line separating the paramagnetic modulated and paramagnetic unmodulated phases is known analytically.[15] The data in the region $\kappa > 0.5$ are taken from the present work; note

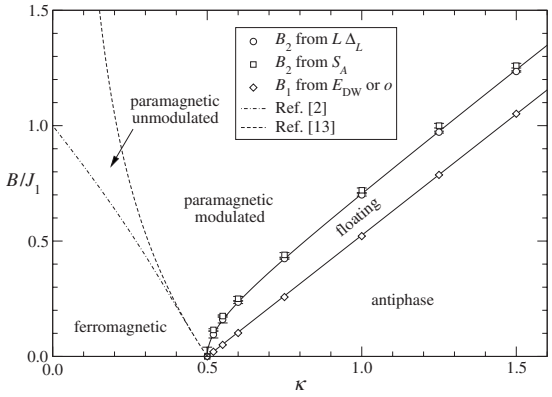

FIG. 16. Phase diagram in the κ-B plane; the solid lines for $\kappa \geqslant 0.5$ correspond to Eq. (18).

that earlier results[3–6] provided only a qualitative picture of the phase diagram in this region.

A very interesting question is whether the floating phase extends up to $\kappa=\infty$ or it terminates at finite κ; we found that the floating phase extends at least up to $\kappa=5$.

VI. SUMMARY AND CONCLUSIONS

We applied the DMRG algorithm to the study of the quantum transverse ANNNI model in the region of high frustration ($\kappa > 0.5$).

We obtained clear evidence for the existence of a floating phase for $\kappa > 0.5$, extending at least up to $\kappa=5$. The floating phase is separated from the paramagnetic modulated phase by a high-order (possibly Kosterliz-Thouless) critical line, ending at the multicritical point ($\kappa=0.5$, $B=0$); the corresponding central charge is $c=1$. In Ref. 7, the floating phase was shown to have a finite extent at $\kappa=0.5$; our study cannot exclude a floating phase of very small extent, i.e., $0 < B_2(\kappa=0.5) \lesssim 0.04$.

We obtained precise estimates for the critical points, verifying that different methods give consistent results. Simple and accurate formulas, for the two critical lines are reported in Eq. (18).

ACKNOWLEDGMENTS

Very helpful discussions with Walter Selke and Pasquale Calabrese are gratefully acknowledged.

*matteo.beccaria@le.infn.it
†massimo.campostrini@df.unipi.it
‡feo@fis.unipr.it

[1] W. Selke, Phys. Rep. **170**, 213 (1998).
[2] M. Beccaria, M. Campostrini, and A. Feo, Phys. Rev. B **73**, 052402 (2006).
[3] Ph. Duxbury and M. Barber, J. Phys. A **14**, L251 (1981).
[4] C. M. Arizmendi, A. H. Rizzo, L. N. Epele, and C. A. Garcia Canal, Z. Phys. B: Condens. Matter **83**, 273 (1991).
[5] P. Sen, S. Chakraborty, S. Dasgupta, and B. K. Chakrabarti, Z. Phys. B: Condens. Matter **88**, 333 (1992).
[6] Paulo R. Colares Guimarães, J. A. Plascak, F. C. Sà Barreto, and J. Florencio, Phys. Rev. B **66**, 064413 (2002).
[7] A. K. Chandra and S. Dasgupta, Phys. Rev. E **75**, 021105 (2007).
[8] P. Calabrese and J. L. Cardy, J. Stat. Mech.: Theory Exp. 0406, P002 (2004).
[9] R. Derian, A. Gendiar, and T. Nishino, J. Phys. Soc. Jpn. **75**, 114001 (2006).
[10] U. Schollwöck, Rev. Mod. Phys. **77**, 259 (2005); see also http://quattro.phys.sci.kobe-u.ac.jp/dmrg.html
[11] http://www.caam.rice.edu/software/ARPACK/
[12] T. Shirahata and T. Nakamura, Phys. Rev. B **65**, 024402 (2001).

[13] Xiao Hu, Prog. Theor. Phys. **89**, 545 (1993); Xiao Hu, J. Phys. A **27**, 2313 (1994).

[14] P. Sen and P. K. Das, in *Quantum Annealing and Related Optimization Methods*, Lecture Notes in Physics 679, edited by A. Das and B. K. Chakrabarti, (Springer, New York, 2005).

[15] I. Peschel and V. J. Emery, Z. Phys. B: Condens. Matter **43**, 241 (1981).

[16] The labels "slow" and "fast" only refer to the different distances involved and have no physical meaning.